Hydrol. Earth Syst. Sci., 18, 2127–2139, 2014
www.hydrol-earth-syst-sci.net/18/2127/2014/
doi:10.5194/hess-18-2127-2014

Hydrology and Earth System Sciences
Open Access

The influence of grid resolution on the prediction of natural and road-related shallow landslides

D. Penna[1,*], M. Borga[1], G. T. Aronica[2], G. Brigandì[2], and P. Tarolli[1]

[1]Department of Land, Environment, Agriculture and Forestry, University of Padova, Agripolis, viale dell'Università 16, 35020 Legnaro (PD), Italy
[2]Department of Civil Engineering, University of Messina, Contrada di Dio, Villaggio S. Agata, 98166 Messina, Italy
[*]now at: Dept. of Environmental Systems Science, Swiss Federal Institute of Technology (ETH), Universitätstrasse 16, 8092, Zurich, Switzerland

Correspondence to: P. Tarolli (paolo.tarolli@unipd.it)

Received: 15 July 2013 – Published in Hydrol. Earth Syst. Sci. Discuss.: 25 July 2013
Revised: 16 April 2014 – Accepted: 22 April 2014 – Published: 10 June 2014

Abstract. This work evaluates the predictive power of the quasi-dynamic shallow landslide model QD-SLaM to simulate shallow landslide locations in a small-scale Mediterranean landscape, namely, the lower portion (2.6 km^2) of the Giampilieri catchment, located in Sicily (Italy). The catchment was impacted by a sequence of high-intensity storms over the years 2007–2009, resulting in widespread landsliding, with a total landslide initiation area amounting to 2.6 % of the basin area. The effect of high-resolution digital terrain models (DTMs) on the quality of model predictions is tested by considering four DTM resolutions: 2, 4, 10 and 20 m. Moreover, the impact of the dense forest road network on the model performance is evaluated by separately considering road-related landslides and natural landslides. The landslide model does not incorporate the description of road-related failures and is applied without calibration of the model parameters. The model predictive power is shown to be DTM-resolution dependent. Use of coarser resolution has a smoothing effect on terrain attributes, with local slope angles decreasing and contributing areas becoming larger. The percentage of watershed area represented by the model as unconditionally unstable (i.e. failing even without the addition of water from precipitation) ranges between 6.3 % at 20 m DTM and 13.8 % at 2 m DTM, showing an overestimation of the mapped landslide area. We consider this prediction as an indication for likely failing sites in future storms rather than areas proved stable during previous storms. When assessed over the sample of mapped non-road-related landslides, better model performances are reported for 4 and 10 m DTM resolution, thus highlighting the fact that higher DTM resolution does not necessarily mean better model performances. Model performances over road-related failures are lower than for the natural cases, and slightly increase with decreasing DTM resolution. These findings indicate that to realize the full potential of high-resolution topography, more extensive work is needed aiming more specifically to identify the extent of the artificial structures and their impact on shallow landsliding processes.

1 Introduction

The occurrence of precipitation-triggered shallow landslides is of concern in hydro-geomorphic and natural hazards science due to the high ranking of such events among natural disasters in terms of both the number of people affected globally and the proportion of fatalities on the affected population. Shallow landsliding can evolve into debris flows, resulting in high risk where vulnerable targets are involved (Petley, 2012).

Landslide susceptibility maps represent one of the key elements for landslide risk management. Landslide susceptibility is the probability that a landslide will occur in a specific area (van Westen, 2000). Quantitative susceptibility assessment is typically accomplished either through the use of empirical models (e.g. Baeza and Corominas, 2001; Lee et al., 2003; Fell et al., 2008), or spatially distributed process-based models of slope stability and hydrology (e.g. Montgomery

and Dietrich, 1994; Casadei et al., 2003; Frattini et al., 2009). A number of recent process-based susceptibility models combine steady-state or quasi-steady-state hydrology concepts with the infinite-slope stability model to calculate the critical rainfall – i.e. the rainfall required to initiate a landslide (e.g. Montgomery et al., 1998; Burton and Bathurst, 1998; Borga et al., 2002; Claessens et al., 2005; Rosso et al., 2006). One of the most important factors controlling the landslide location is surface topography through slope and concentration of shallow subsurface flow (Borga et al., 2002; Penna et al., 2011). Other relevant factors are rainfall intensity and soil and vegetation properties.

Digital terrain model (DTM) resolution affects the calculation of critical rainfall (Zhang and Montgomery, 1994; Claessens et al., 2005; Tarolli and Tarboton, 2006). The last few years have been characterized by the development of new remotely sensed technologies for mapping and analysis of the surface topography (e.g. LiDAR) (Tarolli, 2014). Through high-resolution topography it is possible to recognize in detail local variations in hillslope and valley morphology, and better detect the landslide locations (Lin et al., 2013). However, Zhang and Montgomery (1994) suggested that a resolution of 10 m would be enough for DTM-based geomorphic and hydrological modelling. Similarly, Tarolli and Tarboton (2006) noticed that a very high-resolution DTM might decrease the performance of a shallow landslide model. These findings suggest that such processes are better represented by a smoother topography, which may provide a more realistic approximation of water table distribution than very detailed ones (Freer et al., 2002; Lanni et al., 2013). However, De Sy et al. (2013) noted that for a small-scale catchment in New Zealand, landslide locations were better distinguished from stable areas by using the 1 m resolution topography than coarser resolutions. Contrary to earlier approaches, these authors calibrated the model for each of the DTM resolutions they tested.

Given the advances in high-quality digital elevation data and the lack of guidance, it is desirable to investigate the effect of DTM resolution on the performances of landslide models. Tarolli and Tarboton (2006) reported that one of the reasons for the reduced discriminating capability at fine (< 10 m) DTM resolution was the excessive detail in the surface features, leading to unrepresentative values of terrain slopes. Additionally, there might be other error sources. For instance, a specific error source that arises when using LiDAR elevation data is related to the presence of small-scale artificial structures, such as roads. Road networks and their associated earthworks and drainage structures often result in significant changes to hydrologic and geomorphic responses (Luce, 2002; Dutton et al., 2005). In steep terrain prone to landsliding, roads and the associated drainage structures may significantly impact on the surface/subsurface flow pathways, thus influencing the landsliding potential (Montgomery, 1994; Wemple et al., 2001; Borga et al., 2004; Tarolli et al., 2013). For example, Miller and Burnett (2007) documented a density of road-related landslides double than that of natural surface failures. Specific models have been developed to account for the potential of forest roads to modify landsliding susceptibility (Borga et al., 2004; Dutton et al., 2005). However, we consider here generic models, which are not extended to include road-related processes. This is often the case in practical situations of shallow landslide susceptibility assessment, given the data-intensive characteristics of the road-related model applications (Borga et al., 2004).

The presence of a forest road network may affect the analysis of the predictive power of a shallow landslide model, depending on the DTM resolution. Firstly, a number of observed landslides, used for model assessment, may reflect road-related influences (Montgomery et al., 1998). An error may occur when the model predicts that these landslides are not likely to occur. Caution should be used when considering these errors to assess the model predictive power for road-free areas. Secondly, the high-resolution digital topography reflecting the existing road features may alter model predictions of landslide likelihood. An error may occur when these predictions do not match the mapped failures. This error is mostly influenced by DTM resolution, since road-geometry features cannot be recognized in a coarse-resolution DTM. Also in this case, this kind of error should not be used to assess model performances in road-free areas.

The objective of this work is to investigate the predictive power of a quasi-dynamic process-based landslide model (Borga et al., 2002) in a high-resolution landscape, as a function of the DTM resolution and by considering the specific impact of forest roads. Examination of the DTM resolution sensitivity of process-based shallow landsliding models has received considerable attention in the literature and the distribution of the landsliding susceptibility proved to be to some degree dependent on DTM resolution (Claessens et al., 2005; Tarolli and Tarboton, 2006; de Sy et al., 2013). However, to the best of our knowledge, this is the first time that the assessment is focused on a model which uses the quasi-dynamic wetness index to simulate the groundwater dynamics. The landslide susceptibility model is applied and validated by using lidar-derived DTM data at four different resolutions, ranging from 2 to 20 m, on a small size catchment in Sicily (Italy) characterized by a dense forest road network. For this area repeated field surveys provided an accurate inventory of landslide scars that were distinguished between road-related and natural slides. The model performances are quantified separately for the two types of landslides, to clarify the interplay existing between digital topography and process representation.

2 The shallow landslide model

The QD-SLaM model (Borga et al., 2002; Tarolli et al., 2008) is used in this work to predict the spatial distribution of shallow landslide susceptibility. The QD-SLaM model is based

on the coupling of a topography-driven model of subsurface flow with an infinite slope, Mohr–Coulomb failure model to describe the shallow landsliding process. The model may predict duration and intensity of the rainfall required for landslide initiation. The model uses a quasi-dynamic wetness index (QDWI) to predict the spatial distribution of soil saturation in response to a rainfall of specified duration. The QDWI is the ratio between the effective contributing area and the local slope (Borga et al., 2002). The effective contributing area $a(d)$ is the fraction of the total specific contributing area which contributes subsurface flow to the contour segment within a specified drainage period d corresponding to a rainfall duration. This is based on the hypothesis that all precipitation infiltrates and that vertically infiltrating volumes quickly redistribute and produce lateral subsurface flow. The assumption of instantaneous infiltration, which leads to disregarding the effects of infiltration on near-surface pore-pressure distributions and consequent slope stability, is motivated by the observation of the importance of macropores, pipeflow and preferential flow in a large number of landscapes susceptible to shallow landsliding, including the study area. These processes may have a considerable impact on the response timescale of vertical infiltration and lateral groundwater. Decades of work (see the recent review by Beven and Germann (2013), and reference therein) have shown the significance of vertical and lateral flow through soils containing macropores under unsaturated soil conditions. The influence of these processes on the triggering of shallow landslides has been analysed in detail by Krzeminska (2013), as well as by Uchida et al. (2001) and Hencher (2010), among others.

The effective contributing area is computed under the hypothesis of kinematic lateral flow routing (Barling et al., 1994) as follows:

$$c = \frac{K_s \sin\theta}{\varepsilon}, \tag{1}$$

where c is the celerity of subsurface flow, K_s is the saturated hydraulic conductivity, θ is the local slope angle, and ε is the drainable porosity. We assume ε and K_s vertically uniform, such that the celerity of the subsurface flow is independent of time and of the local wetness conditions. Under the assumptions that there is an impeding layer at depth z (corresponding to the soil bedrock interface) and the layer is parallel to the slope, the height h of the water table above the impeding layer, measured perpendicular to the slope, is computed as follows:

$$h(d) = \min\left[\frac{r}{K_s \sin\theta} a(d), z\right], \tag{2}$$

where r is the constant rainfall rate. The subsurface flow discharge per unit contour width $q(d)$ may be computed by using:

$$q(d) = r a(d). \tag{3}$$

This yields a simple model capable of incorporating the combined effect of storm duration and intensity in the dynamics of the groundwater flow. The methodology used for the computation of the quasi-dynamic contributing area is based on a D8 single-flow direction algorithm. The local slope is estimated by a cell-to-cell computation, along the steepest-descended flow path according to the D8 flow direction method (O'Callaghan and Mark, 1984).

Coupling the groundwater model and the infinite slope stability model under the assumption that the failure plane is on the impeding layer (Taylor, 1948; Haefeli, 1948) provides a relationship for the critical rainfall rate $r_c(d)$, in other words the rainfall rate required to trigger slope failure for the specific topographic element. The relationship reads as follows:

$$r_c(d) = \frac{T \sin\theta}{a(d)} \left[\frac{C}{\rho_w g z \cos\theta \tan\varphi} + \left(\frac{\rho_s}{\rho_w} + \frac{W}{\rho_w g z}\right)\left(1 - \frac{\tan\theta}{\tan\varphi}\right)\right], \tag{4}$$

where C combines soil and root cohesion, W is the vegetation surcharge, φ is the internal friction angle of the soil, ρ_s is the wet soil density, ρ_w is the density of water, g is the gravitational acceleration, and T is the soil transmissivity, defined as the product of the saturated lateral hydraulic conductivity K_s and soil thickness. Since root strength produces significant reinforcement in vegetation-covered slopes, the formulation of QD-SLaM includes the effective soil cohesion due to vegetation. However to avoid making assumptions about landslide size, we considered only basal cohesion and not cohesion around the perimeter of the slide. For a predefined storm duration d, Eq. (4) allows the determination of the minimum uniform rainfall r_c needed to cause instability, which is the meaning of the critical rainfall. Equation (4) extends the definition of critical rainfall provided by Montgomery and Dietrich (1994) by removing the assumption of steady rainfall of infinite duration. In the Mediterranean climate, many slides are actually triggered by the transient response of pore pressures to bursts of intense rainfall, which may occur on short timescales of less than one day. By introducing a dynamic drainage area, the QD-SLaM may offer an efficient way to model the subsurface flow response at short temporal scales (Barling et al., 1994). Moreover, the model provides a framework to relate the characteristics of the critical rainfall (rate and duration) to their probability of exceedance. Application of Eq. (4) allows the definition of three slope stability conditions: unconditionally stable, unconditionally unstable and conditionally unstable. A slope is defined as (a) unconditionally stable if it is stable even when it is saturated, (b) unconditionally unstable if it is unstable even when the soil is dry, and (c) conditionally unstable if the slope instability depends on rainfall conditions. One should note that the model, as applied here, does not include the description of the effects of road drainage on surface/subsurface flow dynamics.

2.1 Coupling the slope stability model with the generalized extreme value (GEV) simple scaling model

Equation (4) provides the critical rainfall rate for a precipitation of a given duration, thus offering a way to quantify the return time of the critical rainfall. The variability of storm intensity with duration for a specified frequency level is often represented by the intensity-duration-frequency (IDF) relation. A power function is often used to model the IDF relation (Koutsoyiannis et al., 1998):

$$r_F(d) = \varsigma_F d^{m_F - 1}, \tag{5}$$

where r_F is the rainfall rate which can be exceeded with a probability of (1-F), and ς_F and m_F are model parameters. The scaling properties of the statistical moments of rainfall depths of different durations are used in this work to derive the IDF relationship (Ceresetti et al., 2010). Aronica et al. (2012) showed that a generalized extreme value (GEV) simple scaling model described well the distribution of annual maximum series of rainfall for the study region. The GEV simple scaling distribution of the rainfall rate $r_F(d)$ can be determined as

$$r_F(d) = \zeta_1 \left\{ u + \frac{\alpha}{k} \left[1 - \exp\left(y_{T_r} k \right) \right] \right\} d^{m-1}, \tag{6}$$

where u, α and k are the parameters of the GEV distribution, ζ_1 and m are scaling parameters, y_{T_r} is derived by the following relation:

$$y_{T_\mathrm{r}} = \ln \left[\ln \left(\frac{T_\mathrm{r}}{T_\mathrm{r} - 1} \right) \right] \tag{7}$$

and T_r, recurrence interval, corresponds to the exceedance probability (1-F). The values of the parameters ζ_1 and m can be estimated by linear regression of mean values of annual maxima of precipitation depth against their durations, after log transformation. Combining Eqs. (4) and (6) yields the following equation for the value of y_{T_r}:

$$\exp(y_{T_\mathrm{r}} k) = 1 - \frac{k}{\alpha} \left\{ \frac{T \sin\theta}{a(d)} \left[\frac{C_\mathrm{r} + C_\mathrm{s}}{\rho_\mathrm{w} g z \cos\theta \tan\varphi} + \left(\frac{\rho_\mathrm{s}}{\rho_\mathrm{w}} + \frac{W}{\rho_\mathrm{w} g z} \right) \left(1 - \frac{\tan\theta}{\tan\varphi} \right) \right] \frac{d^{1-\mathrm{m}}}{\varsigma_1} - u \right\}. \tag{8}$$

Based on Eq. (8), the values of $\exp(y_{T_\mathrm{r}} k)$ can be determined for each topographic element and for a given rainfall duration d. Once the values of $\exp(y_{T_\mathrm{r}} k)$ (represented here as Γ) are determined, the value of return period T_r may be computed as follows:

$$\begin{aligned} y_{T_\mathrm{r}} &= \tfrac{1}{k} \ln \Gamma \\ T_\mathrm{r} &= \tfrac{\exp(\exp y_{T_\mathrm{r}})}{\exp(\exp y_{T_\mathrm{r}}) - 1}. \end{aligned} \tag{9}$$

The critical duration d_cr is the rainfall duration, which minimizes the value of y_{T_r} accordingly with Eqs. (8) and (9). The concept of the critical rainfall rate and duration, derived accordingly with Eq. (8), incorporates in a compact way both the topographic control (represented by the parameters of local slope and effective contributing area) and the climate control (represented by parameters ς_1, u, α, k and m) on shallow landsliding.

3 Study area and model application

The work is focused on the lower portion of the Giampilieri catchment (2.6 km^2), located on the Ionic Sea in the northeastern part of Sicily, southeast of the city of Messina (Fig. 1). The topography is very rugged: elevation ranges from 0 to 596 m a.s.l. with an average value of 236 m a.s.l., and an average slope of 28.5°. The geology of the area is characterized by a meta-sedimentary terrain belonging to the Peloritani Belt that represents the westernmost part of the Calabria–Peloritani Arc and by alluvial deposits and Pleistocenic conglomerates. Phyllites and metarenites develop a soil cover especially at medium/low elevations a.s.l. as the result of weathering; the thickness of colluvium is in the range of 0.7–3.0 m (Messina et al., 1996). The climate is typically Mediterranean, with rainfall events (mainly convective) characterized by short duration and high intensity during the wet season (October–April) and few events during the dry season (May–September). The mean annual rainfall is about 970 mm with 84 % in the wet season and about 16 % in the dry season.

The catchment is predominantly rural, with grassland and crop cultivation (46 %) and shrubs and sparse forest (42.4 %) in the upper mountainous part. The floodplain is densely urbanized by the municipality of Giampilieri Superiore village (Aronica et al., 2012). A dense network of forest road is reported for the catchment (Fig. 1). The forest road system has a length of 19.2 km, and a density of 7.4 km km^{-2}. Roads are unpaved; road cuts truncate colluvial fills in topographic hollows and weathered bedrock in noses and divert both surface and subsurface flow into an in-board ditch system that drains through culverts into the valley bottom. The road width ranges between 4 and 6 m. Consequently, at 10 and 20 m DTM the features related to the road network are generally not recognized because of coarse resolution, while at higher resolution the digital topography is affected by the road network.

In the last 10 years, the study area has been impacted by several large storm events, triggering landslides and floods. On 25 October 2007 more than 120 mm of rain fell in less than 3 hours, with 50 % of the recorded rain concentrated in about 20 min (Aronica et al., 2008). A more extreme storm occurred on 1 October 2009, with high intensity rainfall (exceeding 230 mm in 8 hours) on an area of about 60 km^2 around Giampilieri. The event caused more than 500 landslides (mainly soil slides and debris flows), widespread inundation associated with massive erosion and deposition of

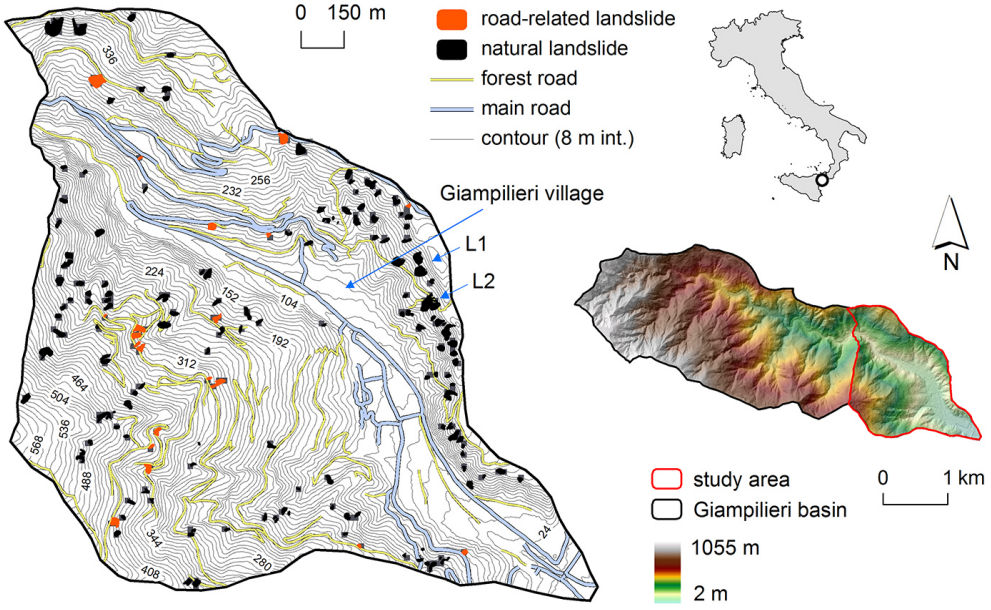

Figure 1. Location map of the study area. Road-related landslides are highlighted in red, while the others are reported in black. The landslides L1 and L2, described as example in Fig. 4, are also reported.

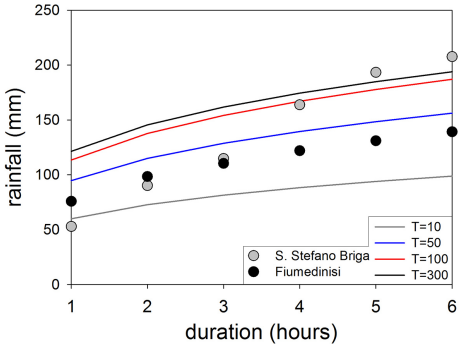

Figure 2. Regional depth-duration-frequency relationship for the study area for return periods ranging from 10 to 300 yr. Observed maxima for rainfall durations ranging from 1 to 6 h measured at the rain gauge stations of S. Stefano and Fiumedinisi during the 2009 event are also reported.

debris along the drainage network. Landslides and inundation caused 31 deaths, 6 missing persons, and an undetermined number of injured people. The evacuees and the homeless people exceeded 2500. Rainfall depths and corresponding durations and return periods for the rainfall data collected at the rain gauges of S. Stefano Briga and Fiumedinisi are reported in Fig. 2, showing that the return period for durations of 5 and 6 hours ranges from 100 to 300 yr. These two rain gauges are located within 6 km of the study basin.

For the study area, a detailed shallow landslide inventory is available (Fig. 1), which includes both landslides triggered by the 2009 event and previous events. The landslides have a rather high length/depth ratio, generally higher than 25. This condition ensures proper application of the infinite length assumption within the infinite slope stability model (Milledge et al., 2012). The landslides were subdivided into road-related and natural slides. Previous investigations (Miller and Burnett, 2007) used a fixed-width buffer on both sides of the road to identify road-related landslides from other slides. In our analysis we examined also the road drainage system features and the coupled hillslope-road topography in order to discriminate road-related landslides. Given the characteristics of the shallow landsliding model used here, which describes only the slope stability processes, only the initiation area is reported for the surveyed landslides. The total landslide initiation area amounts to 67 593 m^2, with 9489 m^2 representing road-related slides. Counter to the conventional wisdom that roads cause the vast majority of shallow slides in steep, soil-mantled catchments (see Gucinski et al., 2001, and references therein), road-related slides account for just 14 % of the mapped slides. This may be due to the catastrophic nature of the event, which caused widespread slope instability in the catchment. Figure 3 provides pictures of two landslides (indicated as L1 and L2 in Fig. 1) just before and after the storm. The figure clearly shows the initiation area as well as the depositional area that impacted the village. The debris flows generated by landslide L1 destroyed or damaged several houses along the creek course, causing several fatalities. Landslide 2 severely impacted the primary school of the village (the school is the large building at the lower boundary of the deposition area). The pictures taken before the storm show that some scars could have been generated by the previous heavy storms that occurred in 2007.

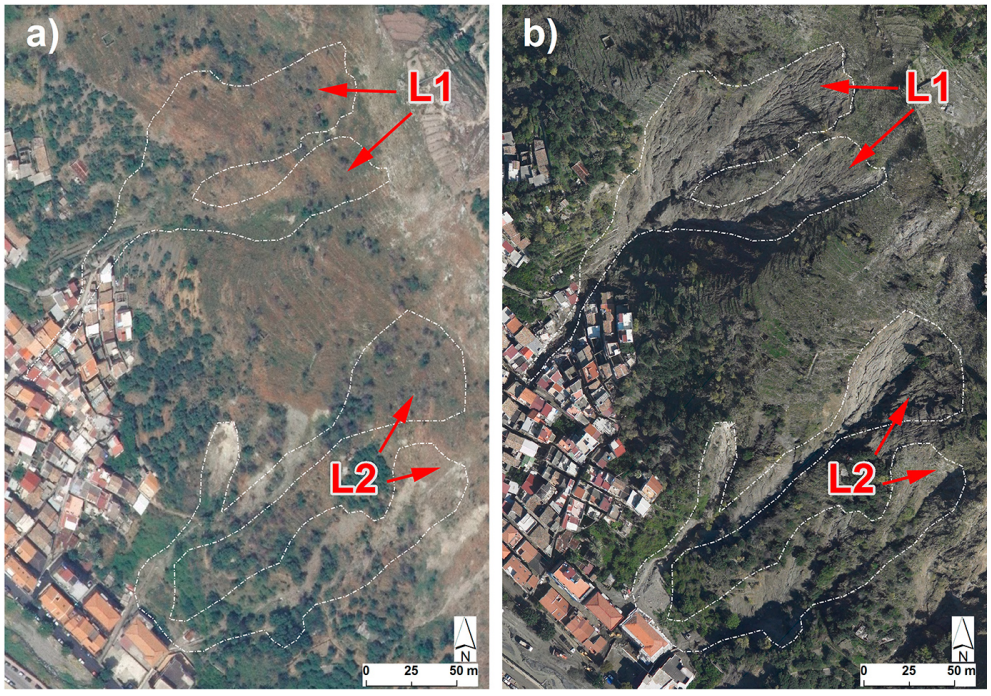

Figure 3. Comparison of aerial photographs taken before **(a)** and after the storm **(b)**, showing landslides L1 and L2, upslope Giampilieri village.

Unlike other works on the topic (Keijsers et al., 2011; De Sy et al., 2013), we decided not to calibrate the landslide model for each DTM resolution considered in the analysis. Recalibrating the model parameters would clearly partially compensate for the changing representation of the morphological attributes associated with each resolution. However, this would also cloud the comparison over the road-related and natural failures, making the examination of the results less straightforward. Instead, we decided to base the model parameterization on the geotechnical and hydraulic parameters obtained from in situ analysis (Regional Department of Civil Protection for Sicily Region, personal communication, 2010). These parameters are reported in Table 1. The influence of vegetation surcharge and root strength on slope stability is confined to a limited portion of the area, where shrubs and forests are widespread. The remaining land is covered by grass which provides some root cohesion. Based on these observations, a value of 1000 Pa, averaged over the basin, is used as combined root and soil cohesion. An average value of soil depth is used, equal to 1 m. The vegetation surcharge was not considered in the analysis since the study area is not covered by forest stands, and the dominant component is grassland. Parameters of the GEV distribution (Table 2) were estimated based on a regional analysis by using the 1, 3, 6, 12 and 24 h duration annual maximum rainfall for a total of 388 station years in a homogeneous region defined accordingly with the L-moment procedures (Hosking an Wallis, 1997), as reported by Aronica et al. (2012).

Table 1. Hydraulic and geotechnical parameters for the study site.

Density ratio (ρ_s/ρ_w)	1.8
Cohesion C (Pa)	1000
Porosity ε (-)	0.35
Friction angle φ (degrees)	35
Saturated hydraulic conductivity K_s ($m\,s^{-1}$)	10^{-3}
Transmissivity T ($m^2\,s^{-1}$)	10^{-3}
Soil depth z (m)	1

The LiDAR-derived DTM at 2 m was regridded on 4, 10 and 20 m grid-cell resolution by using the mean aggregation function in order to obtain coarser digital terrain models. The mean aggregation function was found to ensure a high degree of consistency between surface flow paths extracted from gridded elevation data having different resolutions.

4 Results and discussion

4.1 Influence of DTM resolution on slope, effective specific contributing area and QDWI

To investigate how different DTM resolutions (2, 4, 10 and 20 m) effect the relative shallow landslide susceptibility distribution, the behaviour of three topographic indices derived from the DTM and used in the susceptibility assessment, that is local slope, effective contributing area and QDWI, was

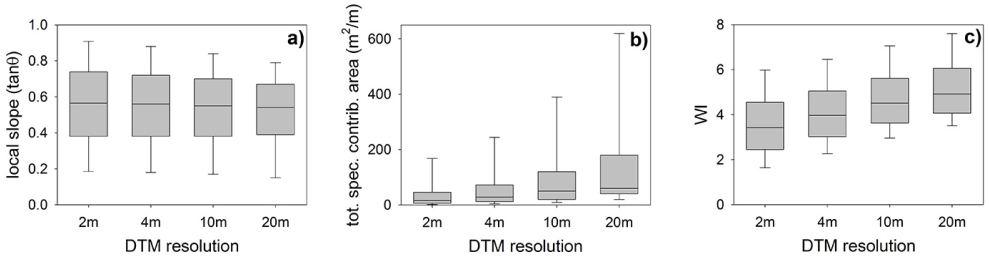

Figure 4. Box plots of topographic attributes for the four different DTM resolutions: **(a)** local slope, **(b)** total specific contributing area, **(c)** WI. The boxes show the 25th and 75th percentile, the whiskers show the 10th and 90th percentile, the horizontal line within the box indicates the median.

Table 2. Parameters estimated for application of GEV model.

Parameter	Value
ζ_1	35.8 mm
α	0.2930
u	0.7550
k	−0.2096
m	0.279

analysed (Figs. 4 and 5). In the figures we show the distribution of both the total (Fig. 4) and the effective (Fig. 5) contributing area, and the relevant wetness indexes. We term here wetness index (WI) as the ratio between the total contributing area and the local slope. Although the total contributing area and WI are not used in QD-SLaM, these topographic attributes represent limiting conditions that help to understand the behaviour of their quasi-dynamic counterparts at very long precipitation durations.

Figure 4a shows the distribution of the slope values for the four DTM resolutions. Although the distributions are similar, it is clear that steep slopes are less represented at the coarser resolutions. The 90th and the 75th percentiles decrease from 0.91 to 0.79 and from 0.74 to 0.67, respectively, with increasing DTM size from 2 to 20 m. On the contrary, the left side of the local slope distribution is almost unaffected by the changes in the DTM resolution.

The distribution of the total specific contributing area (contributing area per unit contour length) for the different resolutions is shown in Fig. 4b. It is possible to observe larger values of specific catchment area for coarser DTM. Similar smoothing effects of coarser resolutions, with contributing areas becoming larger and the local slope angles decreasing, were reported by several researchers for various landscapes (Zhang and Montgomery, 1994; Claessens et al., 2007; Keijsers et al., 2011).

The distribution of the WI for the four resolutions is reported in Fig. 4c. The distribution reflects the behaviour of the specific contributing area and the slope, clearly showing a shift towards higher values with increasing resolution. The 90th and the 75th percentiles increase from 5.98 to 7.60 and from 4.54 to 6.05, respectively, with increasing the DTM size from 2 to 20 m. The distributions of the effective specific contributing area are reported in Fig. 5a–c for the three different durations of 1, 3 and 24 h, respectively, and for the four DTM resolutions. The distributions show that the influence of the resolution increases with the rainfall duration. The distribution of the 24 h-specific contributing area is similar to that reported for the total specific contributing area for the four resolutions. It is interesting to note that, unlike the total case, the minimum specific contributing area values are not directly related to the resolution, since fractions of grid area are computed when the rainfall duration is less than the time taken by the subsurface flow to travel the grid. This is particularly evident for 1 h rainfall duration, where the four distributions exhibit the same behaviour for the right tail and are limited to a range of 1 to 5 m. The distributions of the QDWI are reported in Fig. 5d–f for the three different durations of 1, 3 and 24 h, respectively, and for the four resolutions. The distributions clearly display the smoothing effect related to the decreasing DTM resolution on both slope and effective specific contributing area. Two different patterns emerge. For small rainfall duration (1 and 3 h), the distributions tend be more peaked with decreasing DTM resolution, showing the impact of slope smoothing. For longer rainfall duration (24 h), the distributions are shifted towards larger values with decreasing DTM resolution. Since different rainfall durations are used to generate the critical rainfall return time map, the different sensitivity of the QDWI to the DTM resolution directly translates into a complex pattern of critical rainfall frequency sensitivity to DTM resolution.

4.2 Distribution of the critical rainfall values

The spatial distributions of the critical rainfall frequency are reported in Fig. 6 for the four different DTM resolutions. The Figures show that the main characteristics of the mapped landslides are well represented at the four resolutions, with the observed failures characterized either as unconditionally unstable or with low critical rainfall return period. More specifically, this is the case of the steep valley above the

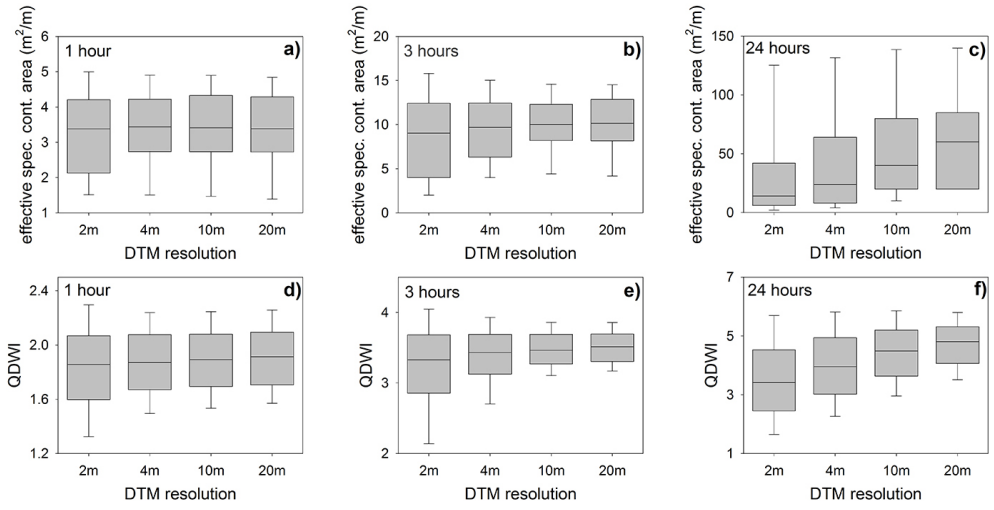

Figure 5. Box plots of topographic attributes for the four different DTM resolutions: **(a)** to **(c)** effective specific contributing area for drainage time ranging from 1 to 24 h, **(d)** to **(f)** QDWI for drainage time ranging from 1 to 24 h. The boxes show the 25th and 75th percentile, the whiskers show the 10th and 90th percentile, the horizontal line within the box indicates the median.

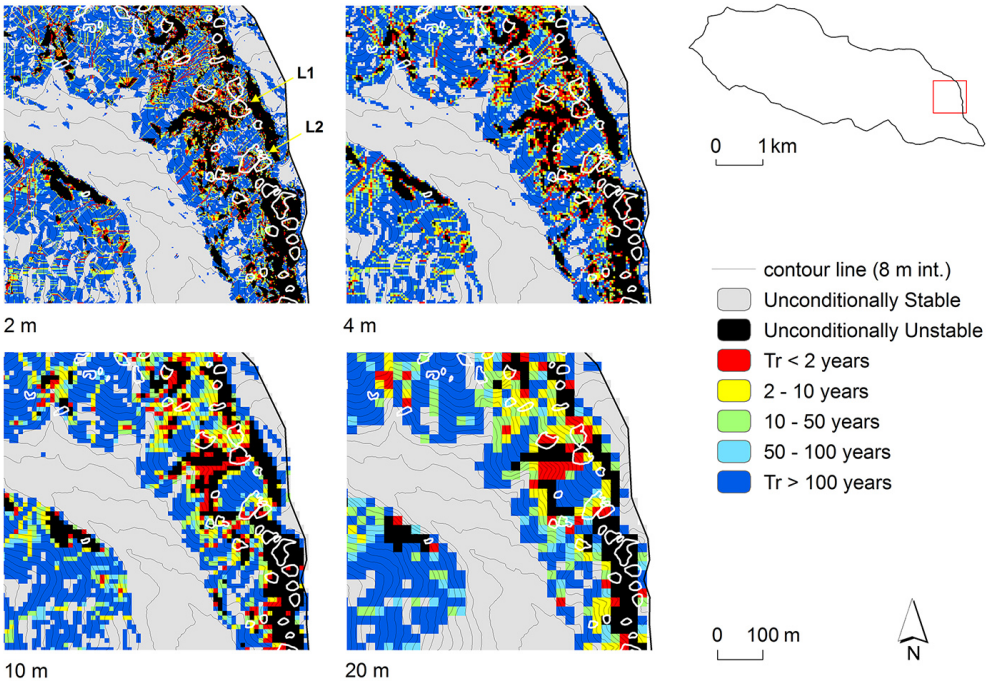

Figure 6. Return period of critical rainfall for four different DTM resolutions: 2, 4, 10, and 20 m (detail of the steep valley above the village of Giampilieri). The landslides are surrounded by white.

village of Giampilieri, on the left side of the creek, where most of the mapped failures are concentrated.

Tables 3 and 4 summarize some key characteristics of the critical rainfall distributions. Table 3 provides the percentages of catchment area and of observed landslide area considered unconditionally unstable and unconditionally stable with the QD-SLaM application for the four DTM resolutions, whereas Table 4 provides the same percentages for two main ranges of critical rainfall frequency. Table 3 shows that more unconditionally unstable cells are reported over the study basin with increasing the DTM resolution, ranging from 6.3 % at 20 m to 13.8 % at 2 m. On the other hand, the percentage of the unconditionally stable cells behaves in a similar way, albeit in a much more reduced range of values, comprised between 30 % at 2 m and 29 % at 20 m. In our application the distribution of unconditionally stable

Table 3. Percentages of catchment area and of observed landslide area considered either unconditionally unstable or unconditionally stable with the QD-SLaM application and for the DTM resolution of 2, 4, 10, and 20 m.

	Catchment area				Landslide area			
	DTM resolution				DTM resolution			
Stability condition	2 m	4 m	10 m	20 m	2 m	4 m	10 m	20 m
Unconditionally unstable	13.75	11.95	9.30	6.34	56.2	52.6	48.0	42.9
Unconditionally stable	30.00	29.77	29.23	29.07	0.	0.	0.	0.

Table 4. Percentages of slope-stability categories in terms of catchment area and of observed landslide area in two main ranges of critical rainfall frequency (return period) for the QD-SLaM application and for the DTM resolution of 2, 4, 10, and 20 m.

	Catchment area				Landslide area			
	DTM resolution				DTM resolution			
Critical rainfall return period	2 m	4 m	10 m	20 m	2 m	4 m	10 m	20 m
< 10 yr	18.3	19.0	18.2	14.1	58.1	70.0	68.7	52.0
≥ 10 yr	81.7	81.0	81.8	85.9	41.9	30.0	31.3	48.0

and unstable states is mainly influenced by local slope. Thus, these effects are related to the distribution of local slope as reported in Fig. 4a, showing a marked impact of the DTM resolution on the higher values of slope, which control the unconditionally unstable condition, and much less on the central values, which control the unconditionally stable condition.

Table 4 shows that the relative frequency of the two main classes of critical rainfall frequency changes in negligible way by varying the DTM resolution from 2 to 10 m. Only for the 20 m DTM do large values of return time increase noticeably. According to Eq. (4), the critical rainfall depends on both the local slope and the QDWI. The results reported in Table 4 imply that the two effects of DTM size on slope and QDWI compensate each other effectively, at least between 2 and 10 m. For a DTM of 20 m the smoothing effect on slope is stronger, thus leading to larger values of critical rain rate and hence of return period.

4.3 Performance assessment methodology

The quality of the model representation of landsliding susceptibility was first assessed by comparing the locations of the observed landslides with those predicted by the model. Better model performance is achieved when a larger difference between fractions of catchment and landslide area corresponding to short recurrence interval of critical rainfall is observed. Tables 3 and 4 report these comparisons for all landslides, without distinction between road-related slides and natural scars.

For a more complete model verification over the three landslide groups (road-related landslides, natural landslides, all landslides), we adopted the assessment methodology developed by Tarolli et al. (2011), which is an extension of the method described above. The methodology can be summarized in a plot where the fraction of basin T_r area $F_B(T_r)$ is reported on the x axis and fraction of landslide T_r area $F_L(T_r)$ on the y axis. The steeper the curve of the plot, the better the performance of the model, because a higher fraction of low T_r area is reported over the observed landslides. The 1 : 1 line represents the "naïve" model, in other words a model without predictive power. The measure of the area below the empirical function is selected here to provide a measure of the model performance. We term this statistic as "efficiency index" (EI). The statistic ranges between 0 and 1, with 1 representing perfect model performances, and 0.5 representing naïve model performances. We examine the model performance for three different set of landslides: (i) road-related slides; (ii) natural slides, and (iii) all landslides, including both road-related and natural slides. Due to the methodology used for the assessment, the comparison is applied only to the conditionally unstable portion of the catchment where the recurrence interval of the critical rainfall is available.

4.4 Evaluation of the model performances at different DTM resolutions

A first assessment is based on results reported in Tables 3 and 4 and concerns all landslides, without distinction between road-related slides and natural failures. Similarly to the results already reported for the basin area (Sect. 4.2), Table 3 shows that more unconditionally unstable cells are predicted over the landslide area with increasing DTM resolution, ranging from 42.9 % at 20 m to 56.2 % at 2 m. This shows again the effect of decreasing slope with coarsening DTM resolution. Interestingly, the percentage of landslide area corresponding to unconditionally stable cells is always

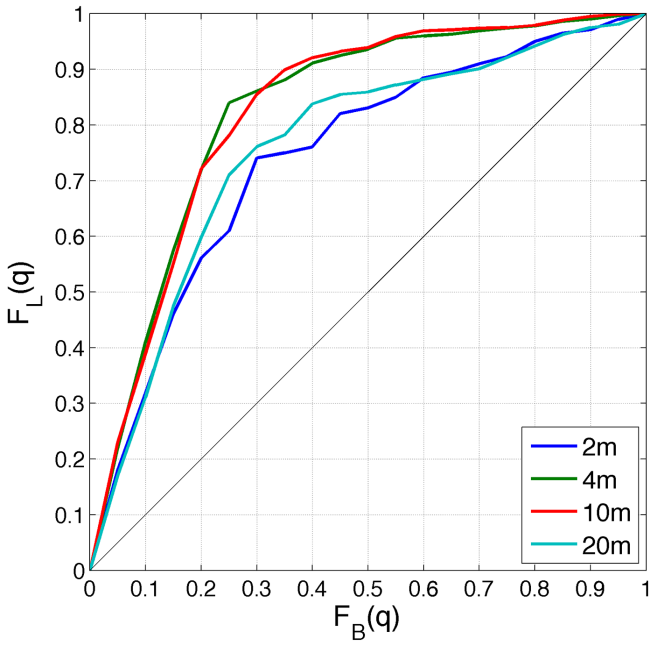

Figure 7. Relationship between cumulative frequencies F_L (q) and F_B (q) considering all landslides and for the DTM resolution of 2, 4, 10, and 20 m. The q variable represents the return period for the QD-SLaM.

zero. The occurrence of mapped landslide in areas predicted to be unconditionally stable is generally considered as an indication about the occurrence of processes external to the model framework (Borga et al., 2002; Tarolli et al., 2011). So, these results show that the processes which are external to the model representation, such as road-related processes, do not emerge over areas considered as unconditionally stable.

Results reported in Table 4, which are weighted on the percentage of area considered as conditionally unstable, offer a first assessment of the DTM resolution impact on the model prediction accuracy. Examination of the results shows that even though the catchment percentages falling into the two main critical rainfall frequencies are roughly similar with coarsening DTM resolution (Table 4), the corresponding spatial organizations of the critical rainfall frequency with respect to the mapped scars are markedly different. Indeed, more landslides are reported in the first range of critical T_r (< 10 yr) for the DTM resolution corresponding to 4 and 10 m, whereas DTMs of 2 and 20 m provide less accurate results, with less landslides reported in the first range of critical T_r. This shows that the 2 and 20 m resolution appear to be of similar poorer quality compared to intermediate resolutions.

Overall, Tables 3 and 4 show that many more cells are predicted to be unconditionally unstable or to fail with moderate rainfall ($T_r < 10$ yr) than are mapped as landslides (which amounts to 2.7 % of the study area). This result is consistent with the general tendency of several process-based models to overestimate the areas predicted as unconditionally unstable or failing with low critical rainfall (Huang and Kao, 2006). Montgomery and Dietrich (1994) reported percentages of unconditionally unstable areas ranging between 1 and 13 %, clearly exceeding the observed landslide area, for the first application of SHALSTAB. In the frame of a more comprehensive validation of SHALSTAB, Dietrich et al. (2001) reported percentages of unconditionally unstable areas ranging between 1 and 23 %, with a mean value of 8 %, for seven well-studied watersheds in northern California. Gorsevski et al. (2006) reported a percentage of 31.2 % for unconditionally unstable areas for a SHALSTAB application in the US. Typically, the assumption of a constant soil depth, usually exceeding the actual one over the steeper portions of the hillslopes, is responsible for this error (Lanni et al., 2012). In our case study, the distribution of soil depth may be affected by a legacy effect due to the presence of terraces. Terraces were built in some steep portions of the basin, by artificially increasing the soil depth distribution. The terraces are now abandoned, hence representing critical conditions for shallow landsliding triggering in unconditionally unstable terrain (Tarolli et al., 2014).

Table 5. Efficiency index for different DTM resolutions and for road-related landslides, natural landslides and for all landslides. Efficiency index equal to 1 represents perfect model performances, and 0.5 represents naïve model performances.

Landslide group	2 m	4 m	10 m	20 m
Road-related	0.54	0.56	0.60	0.61
Natural	0.78	0.87	0.86	0.70
All	0.71	0.82	0.83	0.67

Table 5 reports results in terms of EI for road-related, natural and all landslides and allows for a more complete examination of the interplay between digital topography features and forest roads. Figure 7 provides an example of the comparison when considering all landslides and the four DTM resolutions. Confirming the results shown in Table 4, the statistics reported in Table 5 for all landslides indicate better landslide capability recognition for DTM resolutions corresponding to 4 and 10 m, with relatively high values of EI around 0.83. EI is lower and ranges between 0.67 and 0.71 when considering a DTM of 20 and 2 m, respectively.

The same ranking arises for the natural landslides, with slightly better results. Even in this case, the worst predictions are obtained by using a 20 m DTM (EI = 0.67), whereas predictions with 4 and 10 m DTMs are marked with EI ranging around 0.87.

Model performances over road-related failures are lower than for the natural cases. This is not surprising, given that the QD-SLaM model does not incorporate any module to predict road-related (or other man-related) failures. The model still performs better than the naïve model (characterized by EI = 0.5) because it has a dependence on local

slope, which remains important for road-related landslides. The performances over the road-related failures show a well-defined ranking, with EI decreasing and thus increasing the DTM resolution. This result is likely associated with the increasing impact of the road system on the drainage patterns, for the finer digital topography. At 10 and 20 m resolution, the features related to the road network are not recognized because of coarse resolution, whereas at higher resolution the digital topography is affected by the road network with some likely impact on the computation of the contributing area and slope. More insight on the effect of DTM resolution on road-related failures may be obtained by applying a shallow landsliding model that explicitly recognizes the influence of road-related hydrological processes on shallow landsliding, such as the one developed by Borga et al. (2004). These processes include road interception and re-routing of subsurface flow, and the flow concentration effects due to the road drainage system.

Overall, the results reported here show that caution should be used when assessing the impact of DTM resolution on shallow landslide model predictive power, particularly when the terrain attributes may themselves be dependent on the resolution of the digital topography.

5 Conclusions

In this work a quasi-dynamic shallow landslide model has been applied to the 2.6 km^2 Giampilieri catchment, with the main goal of examining the model predictive power as a function of the DTM resolution. The investigation is carried out separately for road-related landslides and natural landslides. Five main remarks arise from our work.

1. Use of coarser resolution has a smoothing effect on terrain attributes, with local slope angles decreasing and contributing areas becoming larger. However, the effects on the effective contributing areas are shown to be dependent on the precipitation duration, with DTM effects which are negligible for 1 h precipitation and which increase with the duration. This pattern of sensitivity is transmitted to the QDWI. Since the critical rainfall spatial pattern is composed by several precipitation durations, depending on local topography and climate a complex pattern of model sensitivity to the DTM resolution results.

2. The DTM resolution has a remarkable impact on the percentage area considered as unconditionally unstable, which decreases with increasing DTM size. An almost negligible impact is reported for the unconditionally stable areas.

3. Comparison with mapped landslides shows that, even though the catchment percentages falling into the main critical rainfall frequencies are similar when considering both fine and coarse resolutions, the corresponding spatial organizations of the critical rainfall frequency over the mapped scars are markedly different. The model predictive power is shown to be DTM-resolution dependent. When assessed over the sample of mapped natural landslides (i.e. landslides that are not road-influenced), better model performances are reported for 4 and 10 m DTM resolution. This agrees with earlier findings (Tarolli and Tarboton, 2006; Keijsers et al., 2011) and highlights the fact that higher DTM resolution does not necessarily mean better model performance.

4. Model results over the mapped road-related failures outline specific prediction and DTM-sensitivity patterns. Model performance for road-related landslides is worse than for natural landslides. This is not surprising, given that road-related processes are not represented in the model structure. Nevertheless, the model performances are still higher than those corresponding to the naïve model, because it has a dependence on local slope, which remains important for road-related landslides.

5. The model predictive power decreases with increasing DTM resolution, when assessed over the road-related landslides. This is due to the interaction of the model structure (which does not describe the road-related processes) and the impact of road geometry on the digital topography. Model structural error is DTM-resolution neutral and as such it is expected to affect model outcomes independently on DTM resolution. The road impact on digital topography increases with DTM resolution and adds to the error, as shown by the pattern of EI.

Overall, these findings indicate that to realize the full potential of high-resolution topography, more extensive work is needed aiming more specifically at identifying the extent of the artificial structures and their impact on shallow landsliding processes.

Acknowledgements. This research is funded by the Era.Net CICRLE Mountain project ARNICA (10-MCGOT-CIRCLE-2-CVS-185 116). The Regional Department for Civil Protection of Sicily Region is acknowledged for supplying data. The Interdepartmental Research Center of Geomatics (CIRGEO) at the University of Padova is thanked for help in the elaboration of topographic data. The modules of the QD-SLaM model are available at the site: http://intra.tesaf.unipd.it/people/tarolli/Software.htm, software section.

Edited by: T. Bogaard

References

Aronica, G. T., Brigandì, G., Marletta, C., and Manfrè, B.: Hydrological and hydraulic analysis of the flash flood event on 25 October 2007 in North-Eastern part of Sicily, Italy, Proceedings of FLOODrisk 2008, 30 September–2 October 2008, Oxford, UK, 2008.

Aronica, G. T., Brigandí, G., and Morey, N.: Flash floods and debris flow in the city area of Messina, north-east part of Sicily, Italy in October 2009: the case of the Giampilieri catchment, Nat. Hazards Earth Syst. Sci., 12, 1295–1309, doi:10.5194/nhess-12-1295-2012, 2012.

Baeza, C. and Corominas, J.: Assessment of shallow landslide susceptibility by means of multivariate statistical techniques, Earth Surf. Process. Landf., 26, 1251–1263, 2001.

Barling, D. B., Moore, I. D., and Grayson, R. B.: A quasi-dynamic wetness index for characterizing the spatial distribution of zones of surface saturation and soil water content, Water Resour. Res., 30, 1029–1044, 1994.

Beven, K. and Germann, P.: Macropores and water flow in soils revisited, Water Resour. Res., 49, 3071–3092, doi:10.1002/wrcr.20156, 2013.

Borga, M., Dalla Fontana, G., and Cazorzi, F.: Analysis of topographic and climatic control on rainfall-triggered shallow landsliding using a quasi-dynamic wetness index, J. Hydrol., 268, 56–71, 2002.

Borga, M., Tonelli, F., and Selleroni, J.: A physically-based model of the effects of forest roads on slope stability, Water Resour. Res., 40, W12202, doi:10.1029/2004WR003238, 2004.

Burton, A. and Bathurst, J. C.: Physically based modeling of shallow landslide sediment yield at a catchment scale, Environ. Geol., 35, 89–99, 1998.

Casadei, M., Dietrich, W. E., and Miller, N. L.: Testing a model for predicting the timing and location of shallow landslide initiation in soil mantled landscapes, Earth Surf. Process. Landf., 28, 925–950, 2003.

Ceresetti, D., Molinié, G., and Creutin, J.-D.: Scaling properties of heavy rainfall at short duration: A regional analysis, Water Resour. Res., 46, W09531, doi:10.1029/2009WR008603, 2010.

Claessens, L., Heuvelink, G. B. M., Schoorl, J. M., and Veldkamp, A.: DEM resolution effects on shallow landslide hazard and soil redistribution modelling, Earth Surf. Process. Landf., 30, 461–477, 2005.

Claessens, L., Schoorl, J. M., and Veldkamp, A.: Modelling the location of shallow landslides and their effects on landscape dynamics in large watersheds: an application for Northern New Zealand, Geomorphology, 87, 16–27, 2007.

De Sy, V., Schoorl, J. M., Keesstra, S. D., Jones, K. E., and Claessens, L.: Landslide model performance in a high resolution small-scale landscape, Geomorphology, 190, 73–81, 2013.

Dietrich, W. E., Bellugi, D., and Real de Asua, R.: Validation of the shallow landslide model, SHALSTAB, for forest management, in: Land Use and Watersheds: Human influence on hydrology and geomorphology in urban and forest areas, edited by: Wigmosta, M. S. and Burges, S. J., Am. Geoph. Union, Water Science and Application, 2, 195–227, 2001.

Dutton, A. L., Loague, K., and Wemple, B. C.: Simulated effect of a forest road on near-surface hydrologic response and slope stability, Earth Surf. Process. Landf., 30, 325–338, 2005.

Fell, R., Corominas, J., Bonnard, C., Cascini, L., Leroi, E., and Savage, W. Z.: Guidelines for landslide susceptibility, hazard and risk zoning for land-use planning, Eng. Geol., 102, 99–111, 2008.

Frattini, P., Crosta, G., and Sosio, R.: Approaches for defining thresholds and return periods for rainfall-triggered shallow landslides, Hydrol. Process., 23, 1444–1460, 2009.

Gorsevski, P. V., Gessler, P. E., Boll, J., Elliot, W. J., and Foltz, R. B.: Spatially and temporally distributed modeling of landslide susceptibility, Geomorphology, 80, 178–198, 2006.

Gucinski, H., Furniss, M. J., Ziemer, R. R., and Brookes, M. H.: Forest roads: A synthesis of scientific information, Gen. Tech. Rep. PNW-GTR-509, US Dept. of Agric. For. Serv. Pac. Northwest Res. Stat., Portland, Oreg., 103 pp., 2001.

Haefeli, R.: The stability of slopes acted upon by parallel seepage, paper presented at International Conference on Soil Mechanics and Foundation Engineering, 1948.

Hencher, S. R.: Preferential flow paths through soil and rock and their association with landslides, Hydrol. Process., 24, 1610–1630, 2010.

Hosking, J. R. M. and Wallis, J. R.: Regional Frequency Analysis, Cambridge University Press, 224 pp., 1997.

Huang, J. C. and Kao, S. J.: Optimal estimator for assessing landslide model performance, Hydrol. Earth Syst. Sci., 10, 957–965, doi:10.5194/hess-10-957-2006, 2006.

Keijsers, J. G. S., Schoorl, J. M., Chang, K.-T., Chiang, S.-H., Claessens, L., and Veldkamp, A.: Calibration and resolution effects on model performance for predicting shallow landslide locations in Taiwan, Geomorphology, 133, 168–177, 2011.

Koutsoyiannis, D., Kozonis, D., and Manetas, A.: A mathematical framework for studying rainfall intensity-duration-frequency relationships, J. Hydrol., 206, 118–135, 1998.

Krzeminska, D.: The influence of fissures on landslide hydrology, PhD Thesis, University of Delft, 2013.

Lanni, C., Borga, M., Rigon, R., and Tarolli, P.: Modelling shallow landslide susceptibility by means of a subsurface flow path connectivity index and estimates of soil depth spatial distribution, Hydrol. Earth Syst. Sci., 16, 3959–3971, doi:10.5194/hess-16-3959-2012, 2012.

Lanni, C., McDonnell, J., Hopp, L., and Rigon, R.: Simulated effect of soil depth and bedrock topography on near-surface hydrologic response and slope stability, Earth Surf. Process. Landf., 38, 146–159, 2013.

Lee, S. J., Ryu, H., Min, K. D., and Won, J. S.: Landslide susceptibility analysis using GIS and artificial neural network, Earth Surf. Process. Landf., 28, 1361–1376, 2003.

Lin, C. W., Tseng, C.-M., Tseng, Y.-H., Fei, L.-Y., Hsieh, Y.-C., and Tarolli, P.: Recognition of large scale deep-seated landslides in forest areas of Taiwan using high resolution topography, J. Asian Earth Sci., 62, 389–400, 2013.

Luce, C. H.: Hydrological processes and pathways affected by forest roads: What do we still need to learn?, Hydrol. Process., 16, 2901–2904, 2002.

Messina, A., Russo, S., and Stagno, F.: The crystalline basements of the Calabrian-Peloritani Arc. 6th field Meeting IGCP Project no 276, "The Calabrian-Peloritani Arc and its correlation with Northern Africa and Southern Europe", Messina, 27 September–2 October 1993, Newsletter 6, 94 pp., 1996

Milledge, D. G., Griffiths, D. V., Lane, S. N., and Warburton, J.: Limits on the validity of infinite length assumptions for modelling shallow landslides, Earth Surf. Process. Landf. 37, 1158–1166, 2012.

Miller, D. J. and Burnett, K. M.: Effects of forest cover, topography, and sampling extent on the measured density of shallow, translational landslides, Water Resour. Res., 43, W03433, doi:10.1029/2005WR004807, 2007.

Montgomery, D. R.: Road surface drainage, channel initiation, and slope instability, Water Resour. Res., 30, 1925–1932, 1994.

Montgomery, D. R. and Dietrich, W. E.: A physically based model for the topographic control on shallow landsliding, Water Resour. Res., 30, 1153–1171, 1994.

Montgomery, D. R., Sullivan, K., and Greenberg, H. M.: Regional test of a model for shallow landsliding, Hydrol. Process., 12, 943–955, 1998.

Montgomery, D. R., Dietrich, W. E., and Heffner, J. T.: Piezometric response in shallow bedrock at CB1: Implications for runoff generation and landsliding, Water Resour. Res., 38, 10-1–10-18, doi:10.1029/2002WR001429, 2002.

O'Callaghan, J. and Mark, D.: The extraction of drainage networks from digital elevation models, Comput. Vis. Graph. Image Process., 28, 328–344, 1984.

Penna, D., Tromp-van Meerveld, H. J., Gobbi, A., Borga, M., and Dalla Fontana, G.: The influence of soil moisture on threshold runoff generation processes in an alpine headwater catchment, Hydrol. Earth Syst. Sci., 15, 689–702, doi:10.5194/hess-15-689-2011, 2011.

Petley, D. N.: Global patterns of loss of life from landslides, Geology, 40, 927–930, 2012.

Rosso, R., Rulli, M. C., and Vannucchi, G.: A physically based model for the hydrologic control on shallow landsliding, Water Resour. Res., 42, W06410, doi:10.1029/2005WR004369, 2006.

Tarolli, P.: High-resolution topography for understanding Earth surface processes: opportunities and challenges, Geomorphology, 216, 295–312, doi:10.1016/j.geomorph.2014.03.008, 2014.

Tarolli, P. and Tarboton, D. G.: A new method for determination of most likely landslide initiation points and the evaluation of digital terrain model scale in terrain stability mapping, Hydrol. Earth Syst. Sci., 10, 663–677, doi:10.5194/hess-10-663-2006, 2006.

Tarolli, P., Borga, M., and Dalla Fontana G.: Analyzing the influence of upslope bedrock outcrops on shallow landsliding, Geomorphology, 93, 186–200, 2008.

Tarolli, P., Borga, M., Chang, K. T., and Chiang, S. H.: Modeling shallow landsliding susceptibility by incorporating heavy rainfall statistical properties, Geomorphology, 133, 199–211, 2011.

Tarolli, P., Calligaro, S., Cazorzi, F., and Dalla Fontana, G.: Recognition of surface flow processes influeced by roads and trails in mountain areas using high-resolution topography, Eur. J. Remote Sens., 46, 176–197, 2013.

Tarolli, P., Preti, F., and Romano, N.: Terraced landscapes: from an old best practice to a potential hazard for soil degradation due to land abandonment, Anthropocene, doi:10.1016/j.ancene.2014.03.002, in press, 2014.

Taylor, D. W.: Fundamentals of Soil Mechanics, Wiley, New York, 1948.

Uchida, T., Kosugi, K., and Mizuyama, T.: Effects of pipeflow on hydrological process and its relation to landslide: A review of pipeflow studies in forested headwater catchments, Hydrol. Process., 15, 2151–2174, 2001.

van Westen, C. J.: The modeling of landslide hazard using GIS, Surv. Geophys., 21, 241–255, 2000.

Wemple, B. C., Swanson, F. J., and Jones, J. A.: Forest roads and geomorphic process interactions, Cascade Range, Oregon, Earth Surf. Process. Landf., 26, 191–204, 2001.

Zhang, W. and Montgomery, D. R.: Digital elevation model grid size, landscape representation, and hydrologic simulations, Water Resour. Res., 30, 1019–1028, 1994.